

# Stress-Induced Ferroelectricity in Hafnium Oxide Core-Shell Nanoparticles

Anna N. Morozovska<sup>1\*</sup>, Eugene A. Eliseev<sup>2</sup>, Richard (Yu) Liu<sup>3</sup>,  
Sergei V. Kalinin<sup>3†</sup>, and Dean R. Evans<sup>4‡</sup>

<sup>1</sup> Institute of Physics of the National Academy of Sciences of Ukraine, 46, Nauky Avenue, 03028 Kyiv, Ukraine

<sup>2</sup> Frantsevich Institute for Problems in Materials Science of the National Academy of Sciences of Ukraine, 3, str. Omeliana Pritsaka, 03142 Kyiv, Ukraine

<sup>3</sup> Department of Materials Science and Engineering, University of Tennessee, Knoxville, TN, 37996, USA

<sup>4</sup>Zone 5 Technologies, Special Projects Division, San Luis Obispo CA 93401, USA

## Abstract

In contrast to hafnium oxide ( $\text{HfO}_2$ ) thin films, where the appearance of switchable ferroelectric polarization can be induced by strain engineering, reliable methods of ferroelectricity control are absent in  $\text{HfO}_2$  nanoparticles. Direct experimental observations of ferroelectric hysteresis and/or ferroelectric domains, and appropriate modelling of stress-induced ferroelectric states in the nanoparticles are absent too. In this work we study the influence of chemical stresses on phase diagrams and polar properties of spherical  $\text{HfO}_2$  core-shell nanoparticles using the Landau-Ginzburg-Devonshire free energy functional with higher powers, trilinear and biquadratic couplings of polar, antipolar and nonpolar order parameters. It appeared that the ferroelectric phase can be reentrant with respect to the size of nanoparticles, because the spontaneous polarization exists in the limited range of core radii  $R_c$ , namely  $R_{cr}^{min} < R_c < R_{cr}^{max}$ . The minimal critical radius  $R_{cr}^{min}$  is mainly determined by the size dependence of the depolarization field and correlation effects. The maximal critical radius  $R_{cr}^{max}$  is mainly determined by the size dependence of chemical stresses, which are induced by the elastic defects in the shell. Analytical expressions derived for the critical radii can be generalized for hafnium-zirconium oxide nanoparticles, providing that corresponding parameters of the free energy are known from the first principles calculations.

---

\*Corresponding author, e-mail [anna.n.morozovska@gmail.com](mailto:anna.n.morozovska@gmail.com)

† Corresponding author, e-mail [sergei2@utk.edu](mailto:sergei2@utk.edu)

‡ Corresponding author, e-mail: [dean.evans92@gmail.com](mailto:dean.evans92@gmail.com)

## I. INTRODUCTION

Thin films of hafnium-zirconium oxide ( $\text{Hf}_x\text{Zr}_{1-x}\text{O}_2$ ) belong to the most promising silicon-compatible ferroelectric materials for advanced electronics memories [1, 2, 3, 4], and, at the same time, they are ones of the most mysterious, because physical mechanisms responsible for the emergence of ferroelectric and/or antiferroelectric properties are under debate [5, 6]. The transition from the bulk nonpolar monoclinic m-phase (space group  $P2_1/c$ ) to the ferroelectric (FE) orthorhombic o-phase (space group  $Pca2_1$ ) can happen in  $\text{HfO}_2$  films with decrease in thickness  $h$  below the critical value  $h_{cr} \cong 20 - 30$  nm [7], while the FE phase becomes stable in other ferroelectric materials for larger thicknesses,  $h > h_{cr}$ . According to direct experimental observations [8] and ab initio calculations [9, 10], the switching path of spontaneous polarization  $\vec{P}_s$  in thin  $\text{HfO}_2$  films is indirect, at that the transition from  $+\vec{P}_s$  to  $-\vec{P}_s$  states goes through the nonpolar t-phase.

The situation with ferroelectricity existence and polarization switching is much more complicated in small  $\text{Hf}_x\text{Zr}_{1-x}\text{O}_2$  nanoparticles with  $x \geq 0.5$  and sizes  $10 - 30$  nm. Due to the small sizes, it is hardly possible to separate the t-phase (space group  $P4_2/nmc$ ) and o-phases (space groups  $Pbca$ ,  $Pbcm$  and ferroelectric  $Pca2_1$ ) using X-ray diffraction analysis, because corresponding peaks are very close and diffused [11]. In contrast to thin  $\text{HfO}_2$  films, where the appearance of switchable ferroelectric polarization can be induced by strain engineering [12, 13, 14, 15], reliable methods of ferroelectricity control are absent in  $\text{Hf}_x\text{Zr}_{1-x}\text{O}_2$  nanoparticles. Direct experimental observations of ferroelectric hysteresis and/or ferroelectric domains in the nanoparticles are absent too. Since the coupling between polar and nonpolar modes, enhanced by large tensile strains can induce robust ferroelectricity in  $\text{HfO}_2$  thin films [16] and nanoislands [17], similar effects can be expected in  $\text{Hf}_x\text{Zr}_{1-x}\text{O}_2$  nanoparticles. However, the modelling of stress-induced ferroelectric states in the nanoparticles has not been performed yet.

Several experimental [18, 19] and theoretical [20, 21] works revealed a leading role of oxygen vacancies [22, 23] in the appearance and stabilization of the FE o-phase in  $\text{HfO}_2$  thin films. Thermodynamic consideration [24] based on Landau-Ginzburg-Devonshire (LGD) approach predicts that ferro-ionic states can be stable in small  $\text{Hf}_x\text{Zr}_{1-x}\text{O}_2$  nanoparticles due to high screening degree provided by the ionic-electronic charges. It was later shown experimentally, that the oxygen-deficient  $\text{Hf}_x\text{Zr}_{1-x}\text{O}_{2-y}$  nanoparticles, which have a large content of o-phases due to the annealing in  $\text{CO}+\text{CO}_2$  ambient [25, 26], could exhibit ferroelectric-like properties, such as a colossal dielectric response in a wide frequency range [27], as well as demonstrate resistive switching and pronounced charge accumulation [28].

In this work we study the influence of chemical stress on phase diagrams and polar properties

of spherical  $\text{HfO}_2$  nanoparticles with a core-shell structure. For this purpose, we use the LGD free energy functional with higher powers, trilinear and biquadratic couplings of polar, nonpolar and antipolar order parameters [17]. The form of the free energy functional is based on results of Delodovici et al. [29, 30], Jung and Birol [31, 32], who established the principal role of the trilinear coupling. The piezoelectric and electrostriction coupling coefficients of  $\text{HfO}_2$  were determined from Datta et al. results [33]. We derived analytical expressions for the critical sizes of  $\text{HfO}_2$  nanoparticles, which can be generalized for  $\text{Hf}_x\text{Zr}_{1-x}\text{O}_2$  nanoparticles, providing that corresponding parameters of the free energy are known from the first principles calculations.

## II. PROBLEM GEOMETRY AND MAIN ASSUMPTIONS

Let us consider a spherical  $\text{HfO}_2$  core-shell nanoparticle, whose core is assumed to be a single-domain with a spontaneous polarization  $\vec{P}_3$  directed along the polar axis “3”. The core is considered as defect-free, crystalline and insulating. The core is covered with a thin shell, whose thickness  $\Delta R$  is much smaller than  $R_c$ . The core radius is  $R_c$ , and the outer radius is  $R_s = \Delta R + R_c$  (see **Fig. 1(a)**). The shell is assumed to be semiconducting and non-ferroelectric due to the high concentration of free ionic-electronic charges and elastic defects. We assume that the effective screening length in the shell,  $\lambda_{eff}$ , is smaller than the critical value  $\lambda_{cr}$  required for the domain formation in the core. For  $\lambda_{eff} < \lambda_{cr}$  the free charges provide effective screening of the core spontaneous polarization and prevent domain formation, so that the assumption of a single-domain core is self-consistent. The critical value  $\lambda_{cr}$  depends on  $R_c$ ,  $W_s$  and  $T$ . As a rule,  $\lambda_{cr}$  is about 0.1 – 0.5 nm at room temperature and  $R_c \geq 5$  nm. For  $\lambda_{eff} \geq \lambda_{cr}$  one should use the finite element modelling (FEM) [34, 35] or the phase-field approach [36] to account for a possible domain formation in the nanoparticle.

We also assume that the elastic defects in the shell induce strong chemical strains, denoted as  $w_{ij}^s$ . The chemical strains are regarded as isotropic,  $w_{ij}^s = \delta_{ij}w_s$ , where  $\delta_{ij}$  is the Kronecker-delta symbol and  $w_s$  is the magnitude of the strains. These strains, which originated from e.g., oxygen vacancies and/or elastic dipoles, are proportional to the product of Vegard strain tensor  $W_s$  and the defect concentration  $n$ , namely  $w_s \approx W_s n$ . The magnitude of  $W_s$  is about  $(1 - 3) \cdot 10^{-29} \text{ m}^3$  in oxide ferroelectrics [37, 38]. The estimation  $n \approx (1 - 5) \cdot 10^{27} \text{ m}^{-3}$  for the atomic concentration  $n_0 \approx 10^{29} \text{ m}^{-3}$  agrees with many experiments [39, 40, 41, 42], which demonstrate that the defect concentration can exceed 2 – 5 % near the surface of various oxides. Hence, the range of chemical strains  $w_s$  can be taken about 1 – 5 % for the purpose of this work. Due to the elastic mismatch at the core-shell interface, the chemical strains induce elastic stress in the core.

Besides chemical strains, the contribution of the intrinsic surface stress [43] (other name is the

“surface tension”) should be considered. The surface stress contribution is equal to  $-\frac{2\mu}{R_c}$ , where  $\mu$  is the surface tension coefficient and the estimation  $|\mu| \cong 1 - 2 \text{ N/m}$  is valid [44, 45].

The relative dielectric permittivity tensor of the shell,  $\varepsilon_{ij}^s$ , is regarded as cubic,  $\varepsilon_{ij}^s = \delta_{ij}\varepsilon_s$ , and the relative dielectric permittivity  $\varepsilon_s$  can be relatively high due to the paraelectric state of the shell. The core-shell nanoparticle is placed in a paraelectric (e.g.,  $\text{SrTiO}_3$ ,  $\text{KTaO}_3$ ) or dielectric (polymer, gas, liquid, air, or vacuum) ambient with the relative dielectric permittivity  $\varepsilon_e$ . It has been shown [46] that  $\lambda_{eff}$  can be related with the Debye-Hückel length  $L_D$  as  $\lambda_{eff} = \frac{L_D}{\varepsilon_s}$ , where  $L_D = \sqrt{\frac{\varepsilon_0 \varepsilon_s k_B T}{2e^2 n}}$ ,  $\varepsilon_0$  is the vacuum dielectric constant,  $k_B$  is the Boltzmann constant,  $T$  is the absolute temperature and  $e$  is the elementary charge. Block-scheme of the main assumptions is shown in **Fig. 1(b)**.

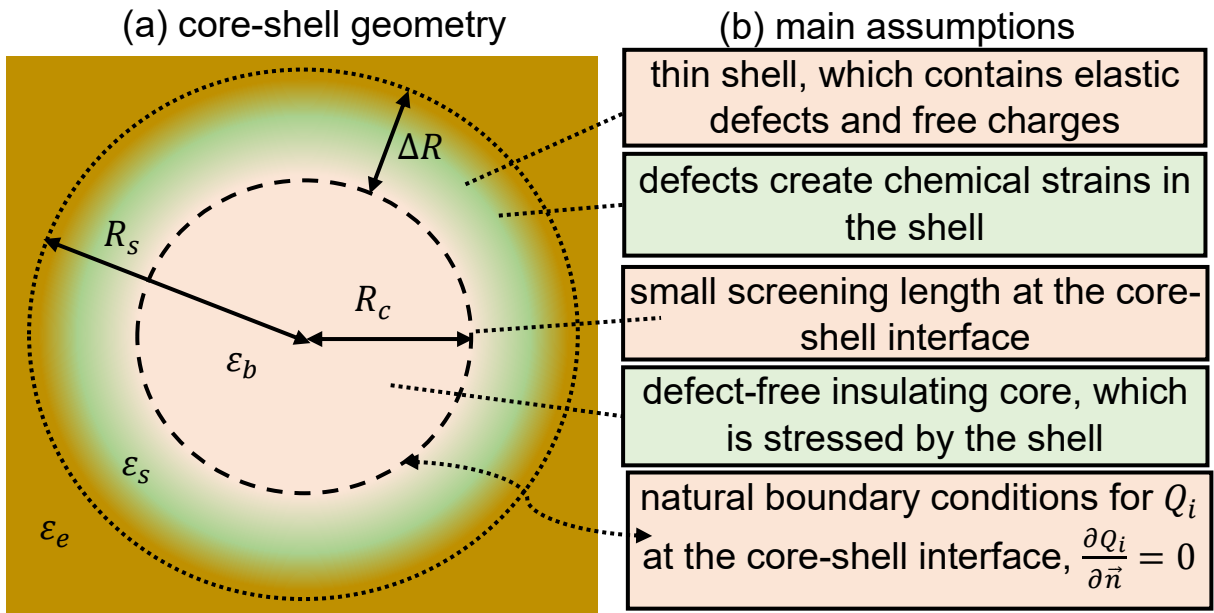


**FIGURE 1.** (a) The cross-section of a spherical  $\text{HfO}_2$  core-shell nanoparticle: a defect-free core of radius  $R_c$  is covered with a paraelectric shell of thickness  $\Delta R$ , which is full of elastic defects and free charges. The nanoparticle is placed in an isotropic dielectric medium;  $\varepsilon_b$ ,  $\varepsilon_s$ , and  $\varepsilon_e$  are the core background, shell, and surrounding media dielectric permittivities. (b) Block-scheme of the main assumptions. The part (a) is adapted from Ref. [48].

### III. THE FREE ENERGY FUNCTIONAL OF $\text{HfO}_2$ CORE-SHELL NANOPARTICLES

The LGD free energy of the  $\text{HfO}_2$  nanoparticle core, corresponding to the FE o-phase  $F_{o\text{-phase}}$ , is the volume integral of the free energy densities  $f_{bulk}$ , electric energy  $f_{el}$  and the surface energy  $F_s$ :

$$F_{o\text{-phase}} = \int (f_{bulk} + f_{el}) dV + F_s, \quad f_{bulk} = f_{bq} + f_{tr} + f_{est} + f_{grad}. \quad (1)$$

The bulk energy density  $f_{bulk}$  is the sum of the biquadratic energy (denoted as  $f_{bq}$ ) and trilinear

coupling energy (denoted as  $f_{tr}$ ) of the polar, antipolar and nonpolar order parameters, elastic and striction energy contributions (denoted as  $f_{est}$ ), and the gradient energy of the order parameters (denoted as  $f_{grad}$ ). The energy  $f_{bq}$  is an expansion over even 2-4-6-8 powers and  $f_{tr}$  is an expansion over odd 3-5-7 powers of the dimensionless amplitudes  $Q_{\Gamma_3}$ ,  $Q_{Y_2}$  and  $Q_{Y_4}$  of the polar phonon mode  $\Gamma_{3-}$ , nonpolar phonon mode  $Y_{2+}$  and antipolar phonon mode  $Y_{4-}$  (see Refs.[17, 29, 30, 31, 32] for details). The energies  $f_{bq}$ ,  $f_{tr}$ ,  $f_{est}$ ,  $f_{grad}$  and  $f_{el}$  are listed in **Supplementary Materials** [47]. In a general case, the surface energy  $F_s$  is the biquadratic form of  $Q_i$ , namely  $F_s = \int \alpha_i Q_i^2 dS$ , where  $Q_i = Q_{\Gamma_3}$ ,  $Q_{Y_2}$  and  $Q_{Y_4}$ . Given the natural boundary conditions at the core-shell interface, namely  $\frac{\partial Q_i}{\partial \vec{n}} = 0$ , the surface energy can be assumed to be zero.

The polarization  $P_3$  is proportional to the amplitude  $Q_{\Gamma_3}$  of the  $\Gamma_{3-}$  mode [17, 30, 31]:

$$P_3 = \frac{Z_B^* d}{V_{f.u.}} Q_{\Gamma_3} \approx P_0 Q_{\Gamma_3}, \quad (2)$$

where  $Z_B^*$  is the effective Bader charge [32],  $d$  is the atomic displacement corresponding to the polar mode,  $V_{f.u.}$  is the formula unit (f.u.) volume,  $P_0$  is the polarization amplitude. The values  $V_{f.u.} \approx 134 \text{ \AA}^3$  and  $P_0 \approx 54.8 \text{ \mu C/cm}^2$  at room temperature [30].

Following Refs.[17, 30], we consider the nonpolar t-phase as the reference “aristo-phase” of the  $\text{HfO}_2$  core. The FE o-phase can be stable in the core when its free energy  $F_{o-phase}$  is smaller than the energy of the m-phase,  $F_m = \int f_m dV$ , where  $f_m \approx -92 \text{ meV/f.u.}$  is the energy density of a bulk  $\text{HfO}_2$  m-phase counted from the t-phase [30]. Thus, the critical sizes of the ferroelectricity appearance/disappearance in the  $\text{HfO}_2$  core-shell nanoparticles can be estimated from the condition

$$F_{o-phase} = F_m. \quad (3)$$

Elastic and/or chemical stresses, surface tension, polarization gradient and depolarization field energies “renormalize” the coefficients in the free energy (1). Elastic stresses  $\sigma_{ij}^c$ , induced by the chemical strain and intrinsic surface stress, have the following form in the nanoparticle core [48]:

$$\sigma_{11}^c = \sigma_{22}^c = \sigma_{33}^c = \frac{-2(R_s^3 - R_c^3)(q_c P_0^2 Q_{\Gamma_3}^2 + z_c Q_{\Gamma_3} Q_{Y_2} Q_{Y_4} - w_s) - 3R_s^3(s_{11}^s + s_{12}^s)^2 \mu}{2(R_s^3 - R_c^3)(s_{11}^c + 2s_{12}^c) + R_s^3(s_{11}^s - s_{12}^s) + 2R_c^3(s_{11}^s + 2s_{12}^s)}. \quad (4)$$

Here,  $s_{ij}^c$  and  $s_{ij}^s$  are the elastic compliances of the core and shell, respectively;  $q_c = (Q_{13}^c + Q_{23}^c + Q_{33}^c)/3$  and  $z_c = (Z_{13}^c + Z_{23}^c + Z_{33}^c)/3$  are the isotropic parts of the electrostriction and trilinear striction tensors of the core, respectively. The non-diagonal stresses are absent,  $\sigma_{12}^c = \sigma_{13}^c = \sigma_{23}^c = 0$ . Note that the contribution of the intrinsic surface stress cannot add more than 0.3 % to the stress of the nanoparticle core with radius  $R_c \geq 5 \text{ nm}$ , since the combination of elastic compliances  $s_{11}^s + 2s_{12}^s$  does not exceed  $3 \cdot 10^{-12} \text{ Pa}^{-1}$  in the  $\text{HfO}_2$  material. For the considered case  $\Delta R \ll R_c$ , the

$$\text{stress } \sigma_{ii}^c \approx \frac{-2\Delta R(q_c P_0^2 Q_{\Gamma 3}^2 + z_c Q_{\Gamma 3} Q_{Y2} Q_{Y4} - w_s)}{R_c(s_{11}^s + s_{12}^s)} - \frac{2\mu}{R_c}.$$

The depolarization field  $E_3^d$  and external field  $E_3^e$  inside the single-domain spherical core with the ferroelectric polarization  $P_3(\vec{r})$  directed along the polar axis “3” have the following form [24]:

$$E_3^d = -\frac{1}{\varepsilon_b + 2\varepsilon_s + (R_c/\lambda_{eff})\varepsilon_0} \frac{P_3}{\varepsilon_0}, \quad E_3^e = \frac{3\varepsilon_e}{\varepsilon_b + 2\varepsilon_s + (R_c/\lambda_{eff})} E_3^0, \quad (5)$$

Hereinafter we suppose that the dielectric permittivity of the shell  $\varepsilon_s$  and the ambient permittivity  $\varepsilon_e$  are close to each other, namely  $\varepsilon_s \approx \varepsilon_e$ .

To derive relatively simple equation for the critical radii of the nanoparticle core, we should assume that the average spontaneous polarization  $\bar{P}_s$  relatively weakly depends on stresses and radius in the “deep” FE o-phase. Using these assumptions and the strong inequality  $\Delta R \ll R_c$ , an approximate algebraic equation for the critical core radius,  $R_{cr}$ , acquires the form:

$$\frac{\lambda_{eff}}{2\varepsilon_0[(\varepsilon_b + 2\varepsilon_s)R_{cr} + \lambda_{eff}]} + \left[ \frac{6\Delta R}{s_{11}^s + s_{12}^s} \left( q_c \bar{P}_s^2 + z_c \bar{Q}_{Y2} \bar{Q}_{Y4} \frac{\bar{P}_s}{P_0} - w_s \right) + \mu \right] \frac{2q_c}{R_{cr}} = -\Delta_\beta, \quad (6)$$

where the positive parameter  $\Delta_\beta$  is estimated at the end of **Supplementary Materials** [47]. If we assume that the parameter  $\Delta_\beta$  is size and stress independent, Eq.(6) becomes a quadratic equation. Under definite conditions it may have two positive roots, denoted as  $R_{cr}^{min}$  and  $R_{cr}^{max}$ .

#### IV. RESULTS AND DISCUSSION

Figures presented below are calculated using exact Eqs.(1)-(5), because the accuracy of approximate Eq.(6) is not high enough near the boundaries between different phases. However, Eq.(6) describes qualitatively the critical sizes of the  $\text{HfO}_2$  core-shell nanoparticles.

The spontaneous polarization  $\bar{P}_s$  and the antipolar order parameter  $\bar{Q}_{Y4s}$  of the  $\text{HfO}_2$  core-shell nanoparticles as a function of defect concentration  $n$  and core radius  $R_c$  are shown in **Fig. 2(a)-2(f)** for several values of the ambient dielectric permittivity  $\varepsilon_e$ :  $\varepsilon_e = 3$  (that corresponds to the low-k ambient),  $\varepsilon_e = 30$  (that corresponds to the high-k polymer) and  $\varepsilon_e = 300$  (that corresponds to the paraelectric  $\text{SrTiO}_3$ ). In the figure we fixed shell thickness  $\Delta R = 1.0$  nm, Vegard tensor magnitude  $W_s = -1 \cdot 10^{-29} \text{ m}^3$  and room temperature  $T = 300$  K. In our calculations we assume that the effective screening length and the chemical strain depend on the defect concentration  $n$  as  $\lambda_{eff} = \sqrt{\frac{\varepsilon_0 k_B T}{2e^2 n \varepsilon_s}}$  and  $w_s \cong W_s n$ , as well as regard that  $\varepsilon_s \cong \varepsilon_e$ .

The FE o-phase can be stable at compressive chemical strains only, namely at  $W_s < 0$ . The urgency to apply compressive strains and to induce the FE o-phase in the  $\text{HfO}_2$  core-shell nanoparticles agrees with DFT results for thin films [14, 17, 30]. The region of the nonpolar m-phase

stability decreases strongly with increase in  $\varepsilon_e$ , being replaced by the FE o-phase (compare the first, the second and the third columns in **Fig. 2**). The FE o-phase is reentrant for  $\varepsilon_e \leq \varepsilon_{max}$  and defect concentrations  $n > n_{min}$ . The maximal value  $\varepsilon_{max} \geq 300$  for material parameters of  $\text{HfO}_2$ ,  $W_s = -1 \cdot 10^{-29} \text{ m}^3$  and room temperature. The minimal concentration of defects,  $n_{min}$ , decreases with increase in  $\varepsilon_e$  from  $2.5 \cdot 10^{27} \text{ m}^{-3}$  at  $\varepsilon_e = 3$  to  $7 \cdot 10^{26} \text{ m}^{-3}$  at  $\varepsilon_e = 300$  (see black circles in **Figs. 2(a), 2(b)** and **2(c)**). Since the depolarization field  $E_3^d \sim \frac{\lambda_{eff}}{(\varepsilon_b + 2\varepsilon_e)R_c + \lambda_{eff}}$  according to Eq.(4), and the effective screening length  $\lambda_{eff} \sim \sqrt{\frac{1}{\varepsilon_e}}$ , the values of  $E_3^d$  and  $\lambda_{eff}$  decreases simultaneously with increase in  $\varepsilon_e$ .

Thus, the simultaneous decrease of the m-phase stability region, minimal concentration  $n_{min}$  and depolarization field  $E_3^d$  is explained by the increase of dielectric and space-charge screening emerging with increase in  $\varepsilon_e$ .

Note that the values of  $\lambda_{eff}$ , which corresponds to the region of FE o-phase stability in **Fig. 2**, are significantly smaller than the critical value  $\lambda_{cr}$  required for the domain formation. The FEM, which consider a possible domain formation, shows that the FE o-phase disappears completely for  $\lambda_{eff} > \lambda_{max}$ , where  $\lambda_{max} > \lambda_{cr}$  and increases with increase in the magnitude of  $W_s$ . It also shows that the domain formation somewhat reduces the critical radius of ferroelectricity disappearance. A detailed consideration of the domain formation in the  $\text{HfO}_2$  core-shell nanoparticles will be presented elsewhere.

Color scale in **Figs. 2(a)-2(c)** is the absolute value of spontaneous polarization  $\bar{P}_s$  in the deepest potential well of the free energy (1). The sharp boundary between the FE o-phase (with  $\bar{P}_s > 0$ ) and nonpolar m-phase (with  $\bar{P}_s = 0$ ) is the first order phase transition curve describing the dependence of the critical radius  $R_{cr}$  on the defect concentration  $n$ . Color scale in **Figs. 2(d)-2(f)** is the absolute value of the antipolar mode  $\bar{Q}_{Y4s}$  in the deepest potential well of the free energy (1).

It is seen from **Figs. 2(g)-2(i)**, that the difference of the antipolar and nonpolar order parameters,  $|\bar{Q}_{Y4s}| - |\bar{Q}_{Y2s}|$ , is very small due to the negligible anisotropy of the deepest potential well as a function of  $|\bar{Q}_{Y4s}|$  and  $|\bar{Q}_{Y2s}|$  [17]. Namely, the difference  $|\bar{Q}_{Y4s}| - |\bar{Q}_{Y2s}|$  does not exceed 0.75 pm, that is more than 30 times smaller than the maximal value of  $\bar{Q}_{Y4s} \approx 0.25 \text{ \AA}$ .

As follows from Eq.(5), the stress-dependent critical core radius of the ferroelectricity appearance (denoted further as  $R_{cr}^{max}$ ) is mainly determined by the size dependence of the chemical stress  $\sigma_{ij}^c$  (proportional to  $\frac{1}{R_{cr}}$  according to Eq.(3)). The critical radius of the ferroelectricity disappearance (denoted further as  $R_{cr}^{min}$ ) is mainly determined by the size dependence of the

depolarization field  $E_3^d$ , proportional to the function  $\frac{\lambda_{eff}}{(\varepsilon_b + 2\varepsilon_s)R_{cr} + \lambda_{eff}}$  according to Eq.(4).

The critical radii,  $R_{cr}^{max}$  and  $R_{cr}^{min}$ , depend on the defect concentration  $n$  and ambient permittivity  $\varepsilon_e$  (see black circles in **Figs. 2(d), 2(e)** and **2(f)**). The radii  $R_{cr}^{min}$  and  $R_{cr}^{max}$  exist at  $n > n_{min}$ ; they become equal at  $n \rightarrow n_{min}$  and disappear at  $n < n_{min}$ . For a wide range of  $\varepsilon_e$ , namely,  $1 \leq \varepsilon_e \leq \varepsilon_{max}$ , the FE o-phase is thermodynamically stable at  $R_{cr}^{min} < R_c < R_{cr}^{max}$  (see black circles in **Figs. 2(d)** and **2(e)**). For large  $\varepsilon_e \geq \varepsilon_{max}$ , the FE o-phase is thermodynamically stable at  $R_c < R_{cr}^{max}$  (see **Fig. 2(f)**). In this case  $R_{cr}^{min}$  is limited by the correlation thickness being equal to several lattice constants.

The deepest minimum of the free energy density,  $f_{o-phase}^{min}$ , as a function of  $n$  and  $R_c$ , calculated for  $\varepsilon_e = 3, 30$  and  $300$ , are shown in **Figs. 2(g), 2(k)** and **2(l)**, respectively. A red background in the figure corresponds to the bulk m-phase with the energy density  $f_m = -92$  meV/f.u. [30]. The first order phase transition between the o-phase and m-phase corresponds to the condition  $f_{o-phase}^{min} = f_m$ . The phase boundary is shown by the black curves in **Figs. 2(g)-2(l)**. As expected, the deepest minimum of  $f_{o-phase}^{min}$  correspond to the large  $n$  and small  $R_c$  (see the top left corner of the diagrams in **Figs. 2(g)-2(l)**).

Similarly to the situation in  $\text{HfO}_2$  thin films considered in Ref. [17], the switching path between the  $-\bar{P}_s$  and  $+\bar{P}_s$  states goes through the virtual  $Ccce$  phase in the  $\text{HfO}_2$  core-shell nanoparticles. Because of this the lowest barrier of polarization switching  $b_{af}$  is about  $+48$  meV/f.u., which corresponds to the energy of the  $Ccce$  phase counted from the t-phase. The activation field  $E_{af}$  of polarization reversal can be estimated as  $E_{af} \cong b_{af}/\bar{P}_s$ , where  $\bar{P}_s$  depends on the chemical strains  $w_s$ , defect concentration  $n$ , core radius  $R_c$  and shell thickness  $\Delta R$ . Color maps of  $E_{af}$  as a function of  $R_c$  and  $n$  are shown in **Figs. 2(m) – 2(o)**. They are calculated for several values of the ambient permittivity  $\varepsilon_e = 3, 30$  and  $300$ . The values of  $E_{af}$  changes from  $0.65$  MV/cm (far from the o-m phase boundary) to  $0.95$  MV/cm (nearby the o-m phase boundary); being very close to the activation fields calculated by us earlier in  $\text{HfO}_2$  thin films [17]. The region of the lowest  $E_{af}$  corresponds to the largest  $n$  and smallest  $R_c$ , because the compressive chemical stress  $\sigma_{ii}^c$  is largest in the region. The region increases with increase in  $\varepsilon_e$  due to depolarization field decrease. The calculated activation fields are somewhat lower than the coercive fields  $E_c \cong 1.05 - 1.35$  MV/cm observed experimentally in 10-nm thick  $\text{HfO}_2$  films [7, 49]. This result is expected from the activation rate theory, because the local nucleation of nanodomains (arising at  $E_3^e \approx E_{af}$ ) precedes the global polarization switching (arising at  $E_3^e \approx E_c$ ).

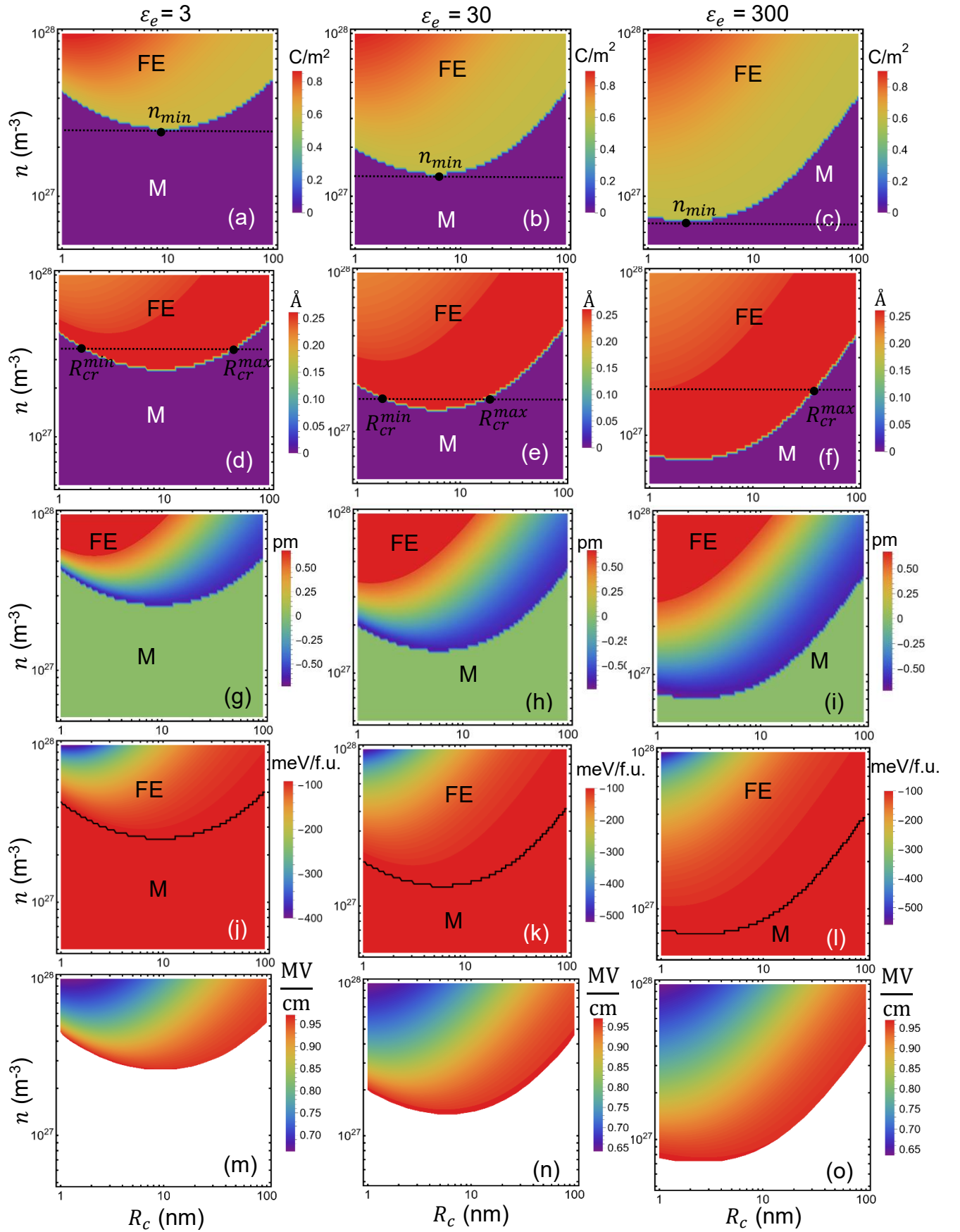


**FIGURE 2.** The absolute value of the spontaneous polarization  $\bar{P}_s$  (a, b, c), the amplitude of the antipolar order

parameter  $|\bar{Q}_{Y4s}|$  (**d**, **e**, **f**), the difference  $|\bar{Q}_{Y4s}| - |\bar{Q}_{Y2s}|$  (**g**, **h**, **i**), the deepest minimum of the free energy density  $f_{o-phase}^{min}$  (**j**, **k**, **l**) and the activation field  $E_{af}$  (**m**, **n**, **o**) as a function of core radius  $R_c$  and defect concentration  $n$  calculated for several values of the ambient permittivity  $\varepsilon_e = 3$  (**a**, **d**, **g**, **j**, **m**), 30 (**b**, **e**, **h**, **k**, **n**) and 300 (**c**, **f**, **i**, **l**, **o**). Abbreviation “FE” is the FE o-phase, “M” denotes the nonpolar m-phase. The shell thickness  $\Delta R = 1$  nm,  $W_s = -1 \cdot 10^{-29}$  m<sup>3</sup>,  $\mu = 0$ ,  $V_{f.u.} \approx 134$  Å<sup>3</sup>,  $T = 300$  K and  $\varepsilon_s \cong \varepsilon_e$ . Material parameters of HfO<sub>2</sub> used in calculations are listed in **Tables S1-S2** in **Appendix S1** of Ref. [17].

## V. CONCLUSIONS

In this work we study the influence of chemical stresses on phase diagrams and polar properties of spherical HfO<sub>2</sub> core-shell nanoparticles using the Landau-Ginzburg-Devonshire free energy functional with higher powers, trilinear and biquadratic couplings of polar, antipolar and nonpolar order parameters.

For not too large values of ambient dielectric permittivity,  $\varepsilon_e \leq \varepsilon_{max}$  the FE o-phase can be reentrant with respect to the size of nanoparticles, which means that the spontaneous polarization exists in the limited range of core radii  $R_c$ , namely  $R_{cr}^{min} < R_c < R_{cr}^{max}$ . The minimal critical radius  $R_{cr}^{min}$  is mainly determined by the size dependence of the depolarization field and correlation effects. The maximal critical radius  $R_{cr}^{max}$  is mainly determined by the size dependence of chemical stresses, which are induced by the elastic defects in the shell. For large  $\varepsilon_e \geq \varepsilon_{max}$ , the FE o-phase is thermodynamically stable at  $R_c < R_{cr}^{max}$  and  $R_{cr}^{min}$  is limited by the correlation thickness being equal to several lattice constants. For chosen material parameters and room temperature  $\varepsilon_{max} \cong 300$ , that corresponds to the SrTiO<sub>3</sub> environment/shell of HfO<sub>2</sub> cores.

We calculated activation fields, which correspond to the local nucleation of nanodomains in the FE o-phase of the HfO<sub>2</sub> core-shell nanoparticles. These fields appeared somewhat lower than the coercive fields observed experimentally in HfO<sub>2</sub> thin films, because the local nucleation precedes the global polarization switching.

Analytical expressions derived for the critical radii can be generalized for hafnium-zirconium oxide nanoparticles, providing that corresponding parameters of the free energy are known from the first principles calculations.

**Acknowledgements.** The work of A.N.M. is funded by the National Research Foundation of Ukraine (project “Manyfold-degenerated metastable states of spontaneous polarization in nanoferroics: theory, experiment and perspectives for digital nanoelectronics”, grant N 2023.03/0132). The work of E.A.E. is funded by the National Research Foundation of Ukraine (project

“Silicon-compatible ferroelectric nanocomposites for electronics and sensors”, grant N 2023.03/0127). The work of S.V.K. is supported by S.V.K. start-up funds. A.N.M. also acknowledges (discussion part) the Horizon Europe Framework Programme (HORIZON-TMA-MSCA-SE), project № 101131229, Piezoelectricity in 2D-materials: materials, modeling, and applications (PIEZO-2D) and the EOARD project 9IOE063 (related STCU partner project is P751c). Numerical results presented in the work are obtained and visualized using a specialized software, Mathematica 14.0 [50].

**Authors’ contribution.** A.N.M. generated the idea of research, formulated the physical problem, performed analytical calculations of the critical size, analyzed results and wrote the manuscript draft. E.A.E. performed symmetry analysis, numerical calculations and prepared corresponding figures. S.V.K. and D.R.E. worked on improvement of the manuscript. All co-authors discussed the results.

## Supplementary Materials

### APPENDIX S1. LGD-type free energy derived from the DFT calculations

The compact form of the LGD free energy bulk density  $f_{bulk}$  is the sum of the 2-4-6-8 powers and 1-5-7 powers of the three phonon modes ( $f_{bl}$  and  $f_{tr}$ ), elastic and striction energy contributions ( $f_{est}$ ), and the gradient energy of the order parameters ( $f_{grad}$ ) [17]:

$$f_{bulk} = f_{bq} + f_{tr} + f_{est} + f_{grad}, \quad (\text{S1.1a})$$

$$f_{bl} = \beta_i Q_i^2 + \delta_{ij} Q_i^2 Q_j^2 + \eta_{ijk} Q_i^2 Q_j^2 Q_k^2 + \xi_{ijkl} Q_i^2 Q_j^2 Q_k^2 Q_l^2, \quad (\text{S1.1b})$$

$$f_{tr} = (\gamma + \epsilon_i Q_i^2 + \zeta_{ij} Q_i^2 Q_j^2) Q_{\Gamma_3} Q_{Y_2} Q_{Y_4}, \quad (\text{S1.1c})$$

$$f_{est} = \frac{1}{2} c_{ijkl} u_{ij} u_{kl} - \tilde{q}_{ijkl} u_{ij} Q_k Q_l - (1 + v_i Q_i^2 + k_{ij} Q_i^2 Q_j^2) \tilde{r}_{ijklm} u_{ij} Q_k Q_l Q_m - \tilde{z}_{ijklmn} u_{ij} Q_k Q_l Q_m Q_n + \tilde{w}_{ijklmn} u_{ij} u_{kl} Q_m Q_n, \quad (\text{S1.1d})$$

$$f_{grad} = \frac{1}{2} g_{ijkl} \frac{\partial Q_k}{\partial x_i} \frac{\partial Q_l}{\partial x_j}. \quad (\text{S1.1e})$$

Here the subscripts  $i, j, k, l, m, n \dots$  either designate the phonon modes  $\Gamma_{3-}$ ,  $Y_{2+}$  and  $Y_{4-}$ , or are the Cartesian indexes coupled to the strains  $u_{ij}$ , or to the Cartesian coordinates  $x_i$ . For instance,  $Q_i$  stands for  $Q_{\Gamma_3}$ ,  $Q_{Y_2}$  or  $Q_{Y_4}$ . The summation rule is performed over repeated subscripts. Following Ref.[30], we pay special attention to the strong trilinear coupling of the  $Q_{\Gamma_3}$ ,  $Q_{Y_2}$  and  $Q_{Y_4}$  amplitudes, which energy  $f_{tr}$  is proportional to the product  $Q_{\Gamma_3} Q_{Y_2} Q_{Y_4}$ , since the coupling can stabilize the FE o-phase.

Nonzero components of  $\beta_i$ ,  $\gamma$ ,  $\delta_{ij}$ ,  $\epsilon_i$ ,  $\eta_{ijk}$ ,  $\zeta_{ij}$  and  $\xi_{ijkl}$  used in calculations for  $\text{HfO}_2$  are listed in **Tables S1-S2** in **Appendix S1** [17].  $c_{ijkl}$  are elastic stiffnesses,  $u_{ij}$  are elastic strains,  $\tilde{q}_{ijkl}$ ,  $\tilde{z}_{ijklmn}$

and  $\tilde{w}_{ijklmn}$  are the components of the second-order and higher-order striction stress tensors;  $\tilde{r}_{ijklm}$  are the tensor of trilinear striction;  $g_{ijkl}$  are the components of the gradient energy tensor.

The ferroelectric polarization components  $P_i$ , both spontaneous and induced by external electric field  $E_i^e$ , contribute to the electric energy  $f_{el}$ :

$$f_{el} = -P_i \left( E_i^e + \frac{1}{2} E_i^d \right). \quad (\text{S1.2a})$$

Here the subscript  $i = 1, 2, 3$  and  $E_i^d$  is the depolarization field, which should be determined from electrostatic equations in a self-consistent way. Following Refs. [30, 31, 32], the ferroelectric polarization  $\vec{P}_3$  is proportional to the amplitude  $Q_{\Gamma 3}$  of the  $\Gamma_{3-}$  mode:

$$P_3 = \frac{Z_B^* d}{V_{f.u.}} Q_{\Gamma 3} \approx P_0 Q_{\Gamma 3}, \quad (\text{S1.2b})$$

where  $Z_B^*$  is the effective Bader charge [32],  $V_{f.u.}$  is the formula unit (f.u.) volume and  $d$  is the elementary displacement corresponding to the polar  $\Gamma_{3-}$  mode. The amplitude of the maximal atomic displacement  $d$  was reported as 0.284, 0.278 and 0.268 Å for the polar, nonpolar and antipolar modes, respectively [30].

Substitution of  $P_3$  in Eqs.(S1.1) instead of  $Q_{\Gamma 3}$ , leads to the rescaling of the coefficients  $\beta_i$ ,  $\gamma$ ,  $\delta_{ij}$ ,  $\epsilon_i$ ,  $\eta_{ijk}$ ,  $\zeta_{ij}$ ,  $\xi_{ijkl}$ ,  $q_{ijkl}$  and  $g_{ijkl}$  proportional to the powers of the factor  $\frac{V_{f.u.}}{Z_B^* d} \approx \frac{1}{P_0}$ . In particular, the biquadratic 2-4-6-8 coupling coefficients  $\tilde{\beta}_{\Gamma 3}$ ,  $\tilde{\delta}_{\Gamma 3}$ ,  $\tilde{\eta}_{\Gamma 3}$ ,  $\tilde{\xi}_{\Gamma 3}$  and the trilinear coupling coefficient  $\tilde{\gamma}$ , responsible for the behavior of the polar mode  $\Gamma_{3-}$ , have the form:

$$\tilde{\beta}_{\Gamma 3} = \frac{\beta_{\Gamma 3}}{P_0^2}, \quad \tilde{\delta}_{\Gamma 3} = \frac{\delta_{\Gamma 3}}{P_0^4}, \quad \tilde{\eta}_{\Gamma 3} = \frac{\eta_{\Gamma 3}}{P_0^6}, \quad \tilde{\xi}_{\Gamma 3} = \frac{\xi_{\Gamma 3}}{P_0^8}, \quad \tilde{\gamma} = \frac{\gamma}{P_0}. \quad (\text{S1.3})$$

## APPENDIX S2. Free energy transformation from fixed strain to zero stress coefficients

Following the first principles calculation of Delodovici et al. [30] we consider the phenomenological free energy at fixed values of strain in the following form

$$\begin{aligned} \Delta F_{FE} = & \zeta \left[ \beta_{\Gamma} \Gamma^2 + \delta_{\Gamma} \Gamma^4 + \eta_{\Gamma} \Gamma^6 + \xi_{\Gamma} \Gamma^8 + (y_{111} - (r_{13}u_1 + r_{23}u_2 + r_{33}u_3)) \Gamma \Psi \Phi + \beta_{\Psi} \Psi^2 + \right. \\ & \delta_{\Psi} \Psi^4 + \eta_{\Psi} \Psi^6 + \xi_{\Psi} \Psi^8 + \beta_{\Phi} \Phi^2 + \delta_{\Phi} \Phi^4 + \eta_{\Phi} \Phi^6 + \xi_{\Phi} \Phi^8 + \delta_{\Gamma \Psi} \Psi^2 \Gamma^2 + \delta_{\Psi \Phi} \Psi^2 \Phi^2 + \\ & \delta_{\Gamma \Phi} \Phi^2 \Gamma^2 + \epsilon_{\Gamma \Psi \Phi} \Gamma^3 \Psi \Phi + \eta_{\Gamma \Psi \Psi} \Gamma^2 \Psi^4 + \eta_{\Gamma \Gamma \Psi} \Gamma^4 \Psi^2 + \eta_{\Gamma \Phi \Phi} \Gamma^2 \Phi^4 + \eta_{\Gamma \Gamma \Phi} \Gamma^4 \Phi^2 + \eta_{\Gamma \Psi \Phi} \Gamma^2 \Psi^2 \Phi^2 + \\ & \left. \xi_{\Gamma \Psi} \Gamma^4 \Psi^4 + \xi_{\Phi \Psi} \Phi^4 \Psi^4 + \xi_{\Gamma \Phi} \Gamma^4 \Phi^4 \right] - \left( E_3^e + \frac{E_3^d}{2} \right) P_0 \Gamma - (q_{13}u_1 + q_{23}u_2 + q_{33}u_3) P_0^2 \Gamma^2 - \\ & (y_{133}u_1 + y_{233}u_2 + y_{333}u_3) P_0^4 \Gamma^4 + \frac{1}{2} (c_{11}u_1^2 + c_{22}u_2^2 + c_{33}u_3^2) + (c_{12}u_1u_2 + c_{13}u_1u_3 + \\ & c_{23}u_2u_3) + \frac{1}{2} (c_{66}u_6^2 + c_{55}u_5^2 + c_{44}u_4^2) \end{aligned} \quad (\text{S2.1})$$

Here  $\Gamma = Q_{\Gamma 3}$ ,  $\Psi = Q_{Y 2}$  and  $\Phi = Q_{Y 4}$  are the shortened re-designations for dimensionless polar, antipolar and nonpolar order parameters, respectively (see **Appendix S1**). Note that the LGD

expansion coefficients at given strain tensor are used in Eq.(S2.1).

In Eq.(S2.1) we introduced the scale factor  $\zeta = e/V_{f.u.}$  to transform from the atomic to SI units ( $e$  is the elementary charge and  $V_{f.u.}$  is the volume of the elementary cell). Voight notations are used in Eq.(S2.1):

$$c_{1111} = c_{11}, \quad c_{1122} = c_{12}, \quad c_{1212} = c_{44}, \quad (S2.2a)$$

$$q_{1111} = q_{11}, \quad q_{1122} = q_{12}, \quad (S2.2b)$$

$$u_{11} = u_1, \quad u_{22} = u_2, \quad 2u_{12} = u_6. \quad (S2.2c)$$

Modified Hooke's law can be obtained from the relation  $\sigma_{ij} = \partial(\Delta F_{FE})/\partial u_{ij}$ :

$$\sigma_1 = c_{11}u_1 + c_{12}u_2 + c_{13}u_3 - q_{13}P_0^2\Gamma^2 - y_{133}P_0^4\Gamma^4 - \zeta r_{13}\Gamma\Psi\Phi, \quad (S2.3a)$$

$$\sigma_2 = c_{12}u_1 + c_{22}u_2 + c_{23}u_3 - q_{23}P_0^2\Gamma^2 - y_{233}P_0^4\Gamma^4 - \zeta r_{23}\Gamma\Psi\Phi, \quad (S2.3b)$$

$$\sigma_3 = c_{13}u_1 + c_{23}u_2 + c_{33}u_3 - q_{33}P_0^2\Gamma^2 - y_{333}P_0^4\Gamma^4 - \zeta r_{33}\Gamma\Psi\Phi, \quad (S2.3c)$$

$$c_{44}u_4 = \sigma_4, \quad c_{55}u_5 = \sigma_5, \quad c_{66}u_6 = \sigma_6. \quad (S2.3d)$$

The stress tensor components have the following form for the mechanically free system under hydrostatic pressure:

$$\sigma_1 = \sigma_2 = \sigma_3 = -p, \quad \sigma_4 = \sigma_5 = \sigma_6 = 0. \quad (S2.4)$$

Considering Eqs.(S2.3) and (S2.4), one could find the strain components as follows:

$$u_1 = -p(s_{11} + s_{12} + s_{13}) + Q_{13}P_0^2\Gamma^2 + Y_{133}P_0^4\Gamma^4 + \zeta Z_{13}\Gamma\Psi\Phi, \quad (S2.5a)$$

$$u_2 = -p(s_{22} + s_{12} + s_{23}) + Q_{23}P_0^2\Gamma^2 + Y_{233}P_0^4\Gamma^4 + \zeta Z_{23}\Gamma\Psi\Phi, \quad (S2.5b)$$

$$u_3 = -p(s_{13} + s_{23} + s_{33}) + Q_{33}P_0^2\Gamma^2 + Y_{333}P_0^4\Gamma^4 + \zeta Z_{33}\Gamma\Psi\Phi, \quad (S2.5c)$$

$$u_4 = u_5 = u_6 = 0. \quad (S2.5d)$$

Here we introduced the second-order electrostriction strain coefficients,

$$Q_{13} = s_{11}q_{13} + s_{12}q_{23} + s_{13}q_{33}, \quad (S2.6a)$$

$$Q_{23} = s_{12}q_{13} + s_{22}q_{23} + s_{23}q_{33}, \quad (S2.6b)$$

$$Q_{33} = s_{13}q_{13} + s_{23}q_{23} + s_{33}q_{33}, \quad (S2.6c)$$

the fourth-order electrostriction coefficients,

$$Y_{133} = s_{11}y_{133} + s_{12}y_{233} + s_{13}y_{333}, \quad (S2.7d)$$

$$Y_{233} = s_{12}y_{133} + s_{22}y_{233} + s_{23}y_{333}, \quad (S2.7d)$$

$$Y_{333} = s_{13}y_{133} + s_{23}y_{233} + s_{33}y_{333}, \quad (S2.7d)$$

and the trilinear striction

$$Z_{13} = s_{11}r_{13} + s_{12}r_{23} + s_{13}r_{33}, \quad (S2.8d)$$

$$Z_{23} = s_{12}r_{13} + s_{22}r_{23} + s_{23}r_{33}, \quad (S2.8d)$$

$$Z_{33} = s_{13}r_{13} + s_{23}r_{23} + s_{33}r_{33}. \quad (S2.8d)$$

It is easy to show that  $r_{13}Q_{13} + r_{23}Q_{23} + r_{33}Q_{33} \equiv q_{13}Z_{13} + q_{23}Z_{23} + q_{33}Z_{33}$ .

In Eqs.(S2.6)-(S2.8) we introduced the compliance tensor  $s_{ij}$  as

$$s_{11} = \frac{c_{23}^2 - c_{22}c_{33}}{c_{13}^2 c_{22} - 2c_{12}c_{13}c_{23} + c_{12}^2 c_{33} + c_{11}(c_{23}^2 - c_{22}c_{33})}, \quad s_{12} = \frac{-c_{13}c_{23} + c_{12}c_{33}}{c_{13}^2 c_{22} - 2c_{12}c_{13}c_{23} + c_{12}^2 c_{33} + c_{11}(c_{23}^2 - c_{22}c_{33})}, \quad (\text{S2.9a})$$

$$s_{13} = \frac{c_{13}c_{22} - c_{12}c_{23}}{c_{13}^2 c_{22} - 2c_{12}c_{13}c_{23} + c_{12}^2 c_{33} + c_{11}(c_{23}^2 - c_{22}c_{33})}, \quad s_{22} = \frac{c_{13}^2 - c_{11}c_{33}}{c_{13}^2 c_{22} - 2c_{12}c_{13}c_{23} + c_{12}^2 c_{33} + c_{11}(c_{23}^2 - c_{22}c_{33})}, \quad (\text{S2.9a})$$

$$s_{23} = \frac{-c_{12}c_{13} + c_{11}c_{23}}{c_{13}^2 c_{22} - 2c_{12}c_{13}c_{23} + c_{12}^2 c_{33} + c_{11}(c_{23}^2 - c_{22}c_{33})}, \quad s_{33} = \frac{c_{12}^2 - c_{11}c_{22}}{c_{13}^2 c_{22} - 2c_{12}c_{13}c_{23} + c_{12}^2 c_{33} + c_{11}(c_{23}^2 - c_{22}c_{33})}. \quad (\text{S2.9a})$$

Neglecting higher-order striction terms, the equation of state for polarization could be found from the minimization of Eq.(S2.1) with respect to  $\Gamma$ :

$$\zeta(2\beta_\Gamma\Gamma + 4\delta_\Gamma\Gamma^3 + 6\eta_\Gamma\Gamma^5 + 8\xi_\Gamma\Gamma^7 + [\gamma_{111} - (r_{13}u_1 + r_{23}u_2 + r_{33}u_3)]\Psi\Phi + 2[\delta_{\Gamma\Psi}\Psi^2 + \delta_{\Gamma\Phi}\Phi^2 + \eta_{\Gamma\Psi\Psi}\Psi^4 + \eta_{\Gamma\Phi\Phi}\Phi^4 + \eta_{\Gamma\Psi\Phi}\Psi^2\Phi^2]\Gamma + 3\zeta\epsilon_{\Gamma\Psi\Phi}\Gamma^2\Psi\Phi + 4[\eta_{\Gamma\Gamma\Psi}\Psi^2 + \eta_{\Gamma\Gamma\Phi}\Phi^2 + \xi_{\Gamma\Psi}\Psi^4 + \xi_{\Gamma\Phi}\Phi^4]\Gamma^3 + \dots\Gamma^5) - 2(q_{13}u_1 + q_{23}u_2 + q_{33}u_3)P_0^2\Gamma = E_3^d + E_3^e. \quad (\text{S2.10a})$$

After the substitution of the strain components from Eq.(S2.5) to Eq.(S2.10a) one obtains the expressions for the renormalized equation of state:

$$2[\zeta\beta_\Gamma + (Q_{12} + Q_{23} + Q_{33})P_0^2p]\Gamma + [4\zeta\delta_\Gamma - 2(q_{13}Q_{13} + q_{23}Q_{23} + q_{33}Q_{33})P_0^4]\Gamma^3 + 6\zeta\eta_\Gamma\Gamma^5 + 8\zeta\xi_\Gamma\Gamma^7 + \zeta[\gamma + (Z_{12} + Z_{23} + Z_{33})p]\Psi\Phi + \dots + 3\zeta(\epsilon_{\Gamma\Psi\Phi} - [r_{13}Q_{13} + r_{23}Q_{23} + r_{33}Q_{33}]P_0^2)\Gamma^2\Psi\Phi + (2\zeta\eta_{\Gamma\Psi\Phi} - \zeta^2[r_{13}Z_{13} + r_{23}Z_{23} + r_{33}Z])\Gamma\Psi^2\Phi^2 = E_3^d + E_3^e \quad (\text{S2.10b})$$

### APPENDIX S3. The internal stress induced by the chemical strains in the shell

Due to the strong chemical strains in the shell, the elastic mismatch between the core and shell lattices appears and induces the stresses in the core. Below we calculate the stress induced by the linearized chemical strains (e.g., Vegard strains) in the paraelectric core.

It is convenient to rewrite the modified Hooke's law Eq.(S2.3) as follows:

$$u_1 = s_{11}\sigma_1 + s_{12}\sigma_2 + s_{13}\sigma_3 + Q_{13}P_0^2\Gamma^2 + \zeta Z_{13}\Gamma\Psi\Phi, \quad (\text{S3.1a})$$

$$u_2 = s_{12}\sigma_1 + s_{22}\sigma_2 + s_{23}\sigma_3 + Q_{23}P_0^2\Gamma^2 + \zeta Z_{23}\Gamma\Psi\Phi, \quad (\text{S3.1b})$$

$$u_3 = s_{13}\sigma_1 + s_{23}\sigma_2 + s_{33}\sigma_3 + Q_{33}P_0^2\Gamma^2 + \zeta Z_{33}\Gamma\Psi\Phi, \quad (\text{S3.1c})$$

$$u_4 = s_{44}\sigma_4, \quad u_5 = s_{55}\sigma_5, \quad u_6 = s_{66}\sigma_6. \quad (\text{S3.1d})$$

To find the elastic fields analytically, we use a perturbation approach. As a first step let us consider an isotropic elastic problem, which has a spherical symmetry, being also consistent with the cubic symmetry of the paraelectric core-shell nanoparticle placed in a soft matter matrix. The elastic displacement in a spherical coordinate frame is given by expression,  $\mathbf{U} = \{U_r(r), U_\theta(r), U_\phi(r)\}$ , where  $U_\theta = U_\phi = 0$  for a spherically symmetric case. In this case, the displacement vector satisfies the equation [51]:

$$\text{grad}(\text{div} \mathbf{U}) \equiv \frac{\partial}{\partial r} \frac{1}{r^2} \frac{\partial}{\partial r} (r^2 U_r) = 0. \quad (\text{S3.2})$$

It is seen from Eq.(S3.2), that the following relation takes place,  $\left(\frac{\partial U_r}{\partial r} + 2\frac{U_r}{r}\right) = C_1$ , and therefore the

general solution of Eq.(S3.2) in the particle core (“c”) and shell (“s”) is:

$$U_r^c = C_1 r, \quad U_r^s = C_2 r + \frac{C_3}{r^2}. \quad (\text{S3.3})$$

The strain tensor components are  $u_{rr}^{c,s} = \frac{\partial U_r^{c,s}}{\partial r}$  and  $u_{\theta\theta}^{c,s} = u_{\phi\phi}^{c,s} = \frac{U_r^{c,s}}{r}$ , and their explicit form is

$$u_{rr}^c = u_{\theta\theta}^c = u_{\phi\phi}^c = C_1, \quad u_{rr}^s = C_2 - 2 \frac{C_3}{r^3}, \quad u_{\theta\theta}^s = u_{\phi\phi}^s = C_2 + \frac{C_3}{r^3}. \quad (\text{S3.4})$$

Substituting the solution (S3.4) into the Hooke’s law (S3.1), we obtain the following expressions for the radial stresses:

$$\sigma_{rr}^c = \frac{C_1 - q_c P_3^2 - \zeta z_c \Gamma \Psi \Phi}{s_{11}^c + 2s_{12}^c}, \quad (\text{S3.5})$$

$$\sigma_{rr}^s = \frac{C_2 - w_s - q_s P^2}{s_{11}^s + 2s_{12}^s} - 2 \frac{C_3}{r^3} \frac{1}{s_{11}^s - s_{12}^s} \approx \frac{C_2 - w_s}{s_{11}^s + 2s_{12}^s} - 2 \frac{C_3}{r^3} \frac{1}{s_{11}^s - s_{12}^s}. \quad (\text{S3.6})$$

Here  $s_{ij}^c$  are elastic compliances,  $q_c = (Q_{13}^c + Q_{23}^c + Q_{33}^c)/3$  and  $z_c = (Z_{13}^c + Z_{23}^c + Z_{33}^c)/3$  are the isotropic parts of electrostriction tensors of the core;  $s_{ij}^s$  are elastic compliances,  $q_s = (Q_{13}^s + Q_{23}^s + Q_{33}^s)/3$  is an isotropic part of the electrostriction tensor, and  $w_s$  are the Vegard strains of the shell. When deriving Eq.(S3.11) we neglected the higher order electrostriction contribution and assumed that the electric field and polarization in the core are homogeneous and directed along the polar axis “3”. However, an inhomogeneous stray electric field can exist in the shell, and therefore we consider the total polarization,  $P^2 = P_1^2 + P_2^2 + P_3^2$ , of the shell. Since the screening length  $\lambda_{eff}$  of the shell is small (less than 1 nm) we can neglect the stray field, and thus omit the electrostriction term,  $q_s P^2$ , in the approximate equality in Eq.(S3.6).

The boundary conditions to Eq.(S3.2) are the continuity of radial elastic displacement and normal stress at core-shell interface,  $r = R_c$ ,

$$u_r^c(R_c) = u_r^s(R_c), \quad \sigma_{rr}^c(R_c) = \sigma_{rr}^s(R_c), \quad (\text{S3.7})$$

and the condition of a fixed pressure/tension at the shell surface,  $r = R_s$ ,

$$\sigma_{rr}^s(R_s) = -p. \quad (\text{S3.8})$$

where  $p$  is an external pressure or intrinsic surface tension. The application of the boundary conditions (S3.7), (S3.8) to the solution (S3.3)-(S3.6) yields the system of equations for the constants  $C_i$ :

$$C_1 R_c = C_2 R_c + \frac{C_3}{R_c^2}, \quad (\text{S3.9a})$$

$$\frac{C_2 - w_s}{s_{11}^s + 2s_{12}^s} - 2 \frac{C_3}{R_c^3} \frac{1}{s_{11}^s - s_{12}^s} = \frac{C_1 - q_c P_3^2 - \zeta z_c \Gamma \Psi \Phi}{s_{11}^c + 2s_{12}^c}, \quad (\text{S3.9b})$$

$$\frac{C_2 - w_s}{s_{11}^s + 2s_{12}^s} - 2 \frac{C_3}{R_s^3} \frac{1}{s_{11}^s - s_{12}^s} = -p. \quad (\text{S3.9c})$$

For the sake of simplicity below we assume that the elastic compliances of the core and the shell are the same:  $s_{11}^s = s_{11}^c = s_{11}$  and  $s_{12}^s = s_{12}^c = s_{12}$ . In this case, the solution of Eqs.(S3.9) is:

$$C_1 = q_c P_3^2 + \zeta z_c \Gamma \Psi \Phi - \frac{s_{11} + 2s_{12}}{s_{11} + s_{12}} \frac{2(R_s^3 - R_c^3)}{3R_s^3} (q_c P_3^2 + \zeta z_c \Gamma \Psi \Phi - w_s) - (s_{11} + 2s_{12})p, \quad (\text{S3.10a})$$

$$C_2 = w_s + \frac{s_{11} + 2s_{12}}{s_{11} + s_{12}} \frac{2R_c^3}{3R_s^3} (q_c P_3^2 + \zeta z_c \Gamma \Psi \Phi - w_s) - (s_{11} + 2s_{12})p, \quad (\text{S3.10b})$$

$$C_3 = \frac{s_{11} - s_{12}}{s_{11} + s_{12}} \frac{R_c^3}{3} (q_c P_3^2 + \zeta z_c \Gamma \Psi \Phi - w_s). \quad (\text{S3.10c})$$

The strain tensor components are:

$$u_{rr}^c = u_{\theta\theta}^c = u_{\phi\phi}^c = q_c P_3^2 + \zeta z_c \Gamma \Psi \Phi - \frac{s_{11} + 2s_{12}}{s_{11} + s_{12}} \frac{2(R_s^3 - R_c^3)}{3R_s^3} (q_c P_3^2 + \zeta z_c \Gamma \Psi \Phi - w_s) - (s_{11} + 2s_{12})p, \quad (\text{S3.11})$$

$$u_{rr}^s = w_s + \left( \frac{s_{11} + 2s_{12}}{s_{11} + s_{12}} \frac{2R_c^3}{3R_s^3} - \frac{s_{11} - s_{12}}{s_{11} + s_{12}} \frac{2R_c^3}{3r^3} \right) (q_c P_3^2 + \zeta z_c \Gamma \Psi \Phi - w_s) - (s_{11} + 2s_{12})p, \quad (\text{S3.12})$$

$$u_{\theta\theta}^s = u_{\phi\phi}^s = w_s + \left( \frac{s_{11} + 2s_{12}}{s_{11} + s_{12}} \frac{2R_c^3}{3R_s^3} + \frac{s_{11} - s_{12}}{s_{11} + s_{12}} \frac{R_c^3}{3r^3} \right) (q_c P_3^2 + \zeta z_c \Gamma \Psi \Phi - w_s) - (s_{11} + 2s_{12})p. \quad (\text{S3.13})$$

Non-trivial stress components in the core are

$$\sigma_{rr}^c = \sigma_{\theta\theta}^c = \sigma_{\phi\phi}^c = -p - \frac{2(R_s^3 - R_c^3)}{3R_s^3(s_{11} + s_{12})} (q_c P_3^2 + \zeta z_c \Gamma \Psi \Phi - w_s). \quad (\text{S3.14})$$

It is seen that the stress tensor (S3.14) is equivalent to some hydrostatic pressure, normalized by the mismatch between the shell and the core.

For the case  $p = 0$ , Eq.(S3.14) is simplified as:

$$\sigma_{rr}^c = \sigma_{\theta\theta}^c = \sigma_{\phi\phi}^c = -\frac{2(R_s^3 - R_c^3)}{3R_s^3} \frac{q_c P_3^2 + \zeta z_c \Gamma \Psi \Phi - w_s}{s_{11} + s_{12}} \approx -2 \frac{\Delta R}{R_s} \frac{q_c P_3^2 + \zeta z_c \Gamma \Psi \Phi - w_s}{s_{11} + s_{12}}, \quad (\text{S3.15})$$

where  $\Delta R$  is the shell thickness. The approximate equality is valid for thin shells,  $(R_s - R_c) \ll R_c$ . The nondiagonal stresses are absent,

$$\sigma_{r\theta}^c = \sigma_{r\phi}^c = \sigma_{\phi\theta}^c = 0. \quad (\text{S3.16})$$

In the important case of different elastic compliances of the core and the shell, the rather cumbersome solution of Eqs.(S3.9) can be found. Of particular interest is the stress in the core, which is given by the following expression:

$$\sigma_{rr}^c = \sigma_{\theta\theta}^c = \sigma_{\phi\phi}^c = \frac{-2(R_s^3 - R_c^3)(q_c P_3^2 + \zeta z_c \Gamma \Psi \Phi - w_s) - 3R_s^3(s_{11}^s + s_{12}^s)p}{R_s^3(2s_{11}^c + 4s_{12}^c + s_{11}^s - s_{12}^s) - 2R_c^3(s_{11}^c + 2s_{12}^c - s_{11}^s - 2s_{12}^s)}. \quad (\text{S3.17})$$

After substitution of the stress (S3.14) into Eq.(S2.10b) and elementary transformations, which is equivalent to the substitution,

$$p \rightarrow p - \frac{2(R_s^3 - R_c^3)w_s}{3R_s^3(s_{11} + s_{12})} + \frac{2(R_s^3 - R_c^3)}{3R_s^3(s_{11} + s_{12})} (q_c P_0^2 \Gamma^2 + \zeta z_c \Gamma \Psi \Phi), \quad (\text{S3.18})$$

the following equation for the spontaneous polarization with renormalized coefficients could be obtained:

$$\left[ 2\zeta\beta_\Gamma + \frac{1}{\varepsilon_b + 2\varepsilon_s + (R_c/\lambda_{eff})} \frac{P_0^2}{\varepsilon_0} + 6q_c P_0^2 \left\{ p - \frac{2(R_s^3 - R_c^3)w_s}{3R_s^3(s_{11} + s_{12})} \right\} \right] \Gamma + \left[ 4\zeta\delta_\Gamma - 2(q_{13}Q_{13} + q_{23}Q_{23}) + \right.$$

$$\begin{aligned}
& q_{33}Q_{33})P_0^4 + \frac{2(q_cP_0^2)^2(R_s^3-R_c^3)}{R_s^3(s_{11}+s_{12})} \Big] \Gamma^3 + \zeta \left[ \gamma + 3z_c \left\{ p - \frac{2(R_s^3-R_c^3)w_s}{3R_s^3(s_{11}+s_{12})} \right\} \right] \Psi\Phi + \dots + 3\zeta \left( \epsilon_{\Gamma\Psi\Phi} - \right. \\
& \left. [r_{13}Q_{13} + r_{23}Q_{23} + r_{33}Q_{33}]P_0^2 + z_cq_cP_0^2 \frac{2(R_s^3-R_c^3)}{R_s^3(s_{11}+s_{12})} \right) \Gamma^2\Psi\Phi + \left( 2\zeta\eta_{\Gamma\Psi\Phi} - \zeta^2[r_{13}Z_{13} + r_{23}Z_{23} + \right. \\
& \left. r_{33}Z_{33}] + (\zeta z_c)^2 \frac{2(R_s^3-R_c^3)}{R_s^3(s_{11}+s_{12})} \right) \Gamma\Psi^2\Phi^2 = E_3^e. \quad (S3.19)
\end{aligned}$$

Only renormalized terms are shown. The shell influence on the coefficients (S3.19) is presented by the factor  $\frac{2(R_s^3-R_c^3)}{3R_s^3}$ . The parameter  $\Delta_\beta$ , introduced in Eq.(6) in the main text, can be estimated from Eq.(S3.19) as

$$\Delta_\beta \cong -\frac{\zeta\beta_\Gamma}{P_0^2} - \frac{f_m}{P_0^2}. \quad (S3.20)$$

## References

---

[1] Roadmap on ferroelectric hafnia and zirconia-based materials and devices, *APL Mater.* **11**, 089201 (2023); <https://doi.org/10.1063/5.0148068>

[2] K.-H. Kim, I. Karpov, R. H. Olsson III, D. Jariwala. Wurtzite and fluorite ferroelectric materials for electronic memory, *Nature Nanotechnology* **18**, 422 (2023); <https://doi.org/10.1038/s41565-023-01361-y>

[3] X. Tao, L. Liu, L. Yang and J.-P. Xu, Impacts of HfZrO<sub>2</sub> thickness and anneal temperature on performance of MoS<sub>2</sub> negative-capacitance field-effect transistors. *Nanotechnology*, **32**, 445201 (2021); <https://doi.org/10.1088/1361-6528/ac197a>

[4] A. Paul, G. Kumar, A. Das, G. Larrieu, and S. De. Hafnium oxide-based ferroelectric field effect transistors: From materials and reliability to applications in storage-class memory and in-memory computing. *J. Appl. Phys.* **138**, 010701 (2025); <https://doi.org/10.1063/5.0278057>

[5] N. Afroze, H. Fahrvandi, G. Ren, P. Kumar, C. Nelson, S. Lombardo, M. Tian, et al. Atomic-scale confinement of strongly charged 180° domain wall pairs in ZrO<sub>2</sub>. *arXiv.2507.18920* (2025); <https://doi.org/10.48550/arXiv.2507.18920>

[6] B. Mukherjee, N. S. Fedorova, Jorge Íñiguez-González. Extrinsic nature of the polarization in hafnia ferroelectrics, *arXiv.2508.00372* (2025); <https://doi.org/10.48550/arXiv.2508.00372>

[7] M. H. Park, Y. H. Lee, H. J. Kim, T. Schenk, W. Lee, K. Do Kim, F. P. G. Fengler, T. Mikolajick, U. Schroeder, and C. S. Hwang. Surface and grain boundary energy as the key enabler of ferroelectricity in nanoscale hafnia-zirconia: a comparison of model and experiment. *Nanoscale* **9**, 9973 (2017); <https://doi.org/10.1039/C7NR02121F>

[8] K. Ooe, Y. Shen, K. Shitara, S. Kobayashi. Y. Shimakawa. D. Kan, J. Etheridge. Direct observation of cation-dependent polarisation switching dynamics in fluorite ferroelectrics, (2025); <https://doi.org/10.48550/arXiv.2509.15682>

[9] Y. Qi, K. M. Rabe, Competing phases of HfO<sub>2</sub> from multiple unstable flat phonon bands of an unconventional high-symmetry phase (2024); <https://doi.org/10.48550/arXiv.2412.16792>

---

[10] Y. Qi, S. Singh, and K. M. Rabe. Polarization switching in ferroelectric HfO<sub>2</sub> from first-principles lattice mode analysis. *Phys. Rev. B* **111**, 134106 (2025); <https://doi.org/10.1103/PhysRevB.111.134106>

[11] K. Fujimoto, Y. Sato, Y. Fuchikami, R. Teranishi, and Kenji Kaneko. Orthorhombic-like atomic arrangement in hafnium-oxide-based nanoparticles. *Journal of the American Ceramic Society* **105**, 2823 (2022); <https://doi.org/10.1111/jace.18242>

[12] S. Estandia, N. Dix, J. Gazquez, I. Fina, J. Lyu, M. F. Chisholm, J. Fontcuberta, and F. Sánchez, Engineering ferroelectric f0.5Zr0.5O2 thin films by epitaxial stress, *ACS Appl. Electron. Mater.* **1**, 1449 (2019); <https://doi.org/10.1021/acsaelm.9b00256>

[13] S. Estandia, N. Dix, M. F. Chisholm, I. Fina, and F. Sánchez, Domain-matching epitaxy of ferroelectric Hf0.5Zr0.5O2(111) on La2/3Sr1/3MnO3(001), *Cryst. Growth Des.* **20**, 3801 (2020); <https://dx.doi.org/10.1021/acs.cgd.0c00095>

[14] Y. Tamura, K. Masuda, and Y. Kumagai. On-demand phase-field modeling: Three-dimensional Landau energy for HfO<sub>2</sub> through machine learning. *arXiv preprint arXiv:2512.16207* (2025); <https://doi.org/10.48550/arXiv.2512.16207>

[15] S. Zhou, J. Zhang, and A. M. Rappe. Strain-induced antipolar phase in hafnia stabilizes robust thin-film ferroelectricity. *Science Advances* **8** (47), eadd5953 (2022); <https://doi.org/10.1126/sciadv.add5953>

[16] S. Zhou, J. Zhang, A. M. Rappe, Strain-induced antipolar phase in hafnia stabilizes robust thin-film ferroelectricity. *Science Advances* **8** (47), eadd5953 (2022); <https://doi.org/10.1126/sciadv.add5953>

[17] A. N. Morozovska, E. A. Eliseev, S. V. Kalinin, and M. V. Strikha. Sizes of Ferroelectricity Appearance and Disappearance in Nanosized Hafnia-Zirconia: Landau-type Theory (2025); <https://doi.org/10.48550/arXiv.2601.06267>

[18] S. Kang, W.-S. Jang, A. N. Morozovska, O. Kwon, Y. Jin, Y.H. Kim, H. Bae, C. Wang, S.H. Yang, A. Belianinov, and S. Randolph, Highly enhanced ferroelectricity in HfO<sub>2</sub>-based ferroelectric thin film by light ion bombardment. *Science*, **376**, 731 (2022); <https://doi.org/10.1126/science.abk3195>

[19] K. P. Kelley, A. N. Morozovska, E. A. Eliseev, Y. Liu, S. S. Fields, S. T. Jaszewski, T. Mimura, J. Ihlefeld, S. V. Kalinin. Ferroelectricity in Hafnia Controlled via Surface Electrochemical State. *Nature Materials* **22**, 1144 (2023); <https://doi.org/10.1038/s41563-023-01619-9>

[20] M.D. Glinchuk, A.N. Morozovska, A. Lukowiak, W. Stręk, M.V. Silibin, D.V. Karpinsky, Y.Kim, and S.V. Kalinin. Possible Electrochemical Origin of Ferroelectricity in HfO<sub>2</sub> Thin Films. *Journal of Alloys and Compounds*, **830**, 153628 (2020); <https://doi.org/10.1016/j.jallcom.2019.153628>

[21] L.-Y. Ma and S. Liu. Structural Polymorphism Kinetics Promoted by Charged Oxygen Vacancies in HfO<sub>2</sub>. *Phys. Rev. Lett.* **130**, 096801 (2023); <https://doi.org/10.1103/PhysRevLett.130.096801>

[22] T.K. Paul, A.K. Saha, and S.K. Gupta, Oxygen vacancy-induced monoclinic dead layers in ferroelectric HfO<sub>2</sub> with metal electrodes. *J. Appl. Phys.* **137**, 144102 (2025); <https://doi.org/10.1063/5.0252663>

---

[23] G. Zhang, H. Wu, X. Xu, S. Lin, Z. Zhang, Z. Yan, X. Lu, G. Yuan, and J.-M. Liu. Enhanced reliability of  $\text{Hf}_{0.5}\text{Zr}_{0.5}\text{O}_2$  ferroelectric memory through  $\text{WO}_x$  buffer layer to minimize oxygen vacancies. *Appl. Phys. Lett.* **127**, 112102 (2025); <https://doi.org/10.1063/5.0284623>

[24] E. A. Eliseev, S. V. Kalinin, A. N. Morozovska. Ferro-ionic States and Domains Morphology in  $\text{Hf}_x\text{Zr}_{1-x}\text{O}_2$  Nanoparticles. *Journal of Applied Physics*, **137**, 034103 (2025); <https://doi.org/10.1063/5.0243067>

[25] E. A. Eliseev, Y. O. Zagorodniy, V. N. Pavlikov, O. V. Leshchenko, H. V. Sheviliakova, M. V. Karpec, A. D. Yaremkevych, O. M. Fesenko, S. V. Kalinin, and A. N. Morozovska. Phase diagrams and polarization reversal in nanosized  $\text{Hf}_x\text{Zr}_{1-x}\text{O}_{2-y}$ , *AIP Advances*, **14**, 055224 (2024); <https://doi.org/10.1063/5.0209123>

[26] E. A. Eliseev, I. V. Kondakova, Y. O. Zagorodniy, H. V. Sheviliakova, O. V. Leshchenko, V. N. Pavlikov, M. V. Karpets, L. P. Yurchenko, and A. N. Morozovska, The origin of the ferroelectric-like orthorhombic phase in oxygen-deficient  $\text{HfO}_{2-y}$  nanoparticles. *Semiconductor Physics, Optoelectronics and Quantum Electronics*, **28**, 134 (2025); <https://doi.org/10.15407/spqeo28.02.134>

[27] O. S. Pylypchuk, V. V. Vainberg, V. N. Poroshin, O. V. Leshchenko, V. N. Pavlikov, I. V. Kondakova, S. E. Ivanchenko, L. P. Yurchenko, L. Demchenko, A. O. Diachenko, M. V. Karpets, M. P. Trubitsyn, E. A. Eliseev, and A. N. Morozovska. A colossal dielectric response of  $\text{Hf}_x\text{Zr}_{1-x}\text{O}_2$  nanoparticles. *Physical Review Materials* **9**, 114412 (2025); <https://doi.org/10.1103/y2pb-5g5w>

[28] O. S. Pylypchuk, I. V. Fesych, V. V. Vainberg, Y. O. Zagorodniy, V. I. Styopkin, J. M. Gudenko, I. V. Kondakova, L. P. Yurchenko, V. N. Pavlikov, A. O. Diachenko, M. M. Koptiev, M. D. Volnyanskii, V. V. Laguta, E. A. Eliseev, M. P. Trubitsyn, and A. N. Morozovska. Resistive switching and charge accumulation in  $\text{Hf}_{0.5}\text{Zr}_{0.5}\text{O}_2$  nanoparticles. *Journal of Physical Chemistry* **29**, 31, 14299 (2025); <https://doi.org/10.1021/acs.jpcc.5c04140>.

[29] F. Delodovici, P. Barone, and S. Picozzi. Finite-size effects on ferroelectricity in rhombohedral  $\text{HfO}_2$ . *Phys. Rev. B* **106**, 115438 (2022); <https://doi.org/10.1103/PhysRevB.106.115438>

[30] F. Delodovici, P. Barone, and S. Picozzi, Trilinear-coupling-driven ferroelectricity in  $\text{HfO}_2$ , *Physical Review Materials* **5**, 064405 (2021); <https://doi.org/10.1103/PhysRevMaterials.5.064405>

[31] S. Jung and T. Birol, Triggered ferroelectricity in  $\text{HfO}_2$  from hybrid phonons, *arXiv:2502.08633* (2025); <https://doi.org/10.48550/arXiv.2502.08633>

[32] S. Jung and T. Birol, Electric Polarization from Nonpolar Phonons, *arXiv: 2512.00628* (2025); <https://doi.org/10.48550/arXiv.2512.00628>

[33] S. Dutta, P. Buragohain, S. Glinsek, C. Richter, H. Aramberri, H. Lu, U. Schroeder, E. Defay, A. Gruverman, J. Íñiguez. Piezoelectricity in hafnia. *Nature Communications* **12**, 7301 (2021); <https://doi.org/10.1038/s41467-021-27480-5>

[34] Y.A. Genenko, O. Hirsch, and P. Erhart, Surface potential at a ferroelectric grain due to asymmetric screening of depolarization fields, *J. Appl. Phys.* **115**, 104102 (2014); <https://doi.org/10.1063/1.4867984>

---

[35] I. S. Vorotiahin, E. A. Eliseev, Q. Li, S. V. Kalinin, Y. A. Genenko and A. N. Morozovska. Tuning the Polar States of Ferroelectric Films via Surface Charges and Flexoelectricity. *Acta Materialia* **137**, 85 (2017) <https://doi.org/10.1016/j.actamat.2017.07.033>

[36] J.-J. Wang, B. Wang, and L.-Q. Chen. Understanding, Predicting, and Designing Ferroelectric Domain Structures and Switching Guided by the Phase-Field Method. *Ann. Rev. Mater. Res.* **49**, 127 (2019). <https://doi.org/10.1146/annurev-matsci-070218-121843>

[37] D. A. Freedman, D. Roundy, and T. A. Arias. Elastic effects of vacancies in strontium titanate: Short- and long-range strain fields, elastic dipole tensors, and chemical strain. *Phys. Rev. B* **80**, 064108 (2009), <https://doi.org/10.1103/PhysRevB.80.064108>

[38] Y. Kim, A. S. Disa, T. E. Babakol, and J. D. Brock. Strain screening by mobile oxygen vacancies in  $\text{SrTiO}_3$ . *Appl. Phys. Lett.* **96**, 251901 (2010), <https://doi.org/10.1063/1.3455157>

[39] S. Bourgeois, B. Domenichini and J. Jupille, Excess Electrons at Oxide Surfaces, Chapter 4 in: Defects at Oxide Surfaces, ed.: J. Jupille and G. Thornton, Springer Series in Surface Sciences 58, (2015), [https://doi.org/10.1007/978-3-319-14367-5\\_4](https://doi.org/10.1007/978-3-319-14367-5_4)

[40] M.J. Highland, T.T. Fister, D.D. Fong, P.H. Fuoss, C. Thompson, J.A. Eastman, S.K. Streiffer, and G.B. Stephenson. Equilibrium polarization of ultrathin  $\text{PbTiO}_3$  with surface compensation controlled by oxygen partial pressure. *Phys. Rev. Lett.* **107**, 187602 (2011). <https://doi.org/10.1103/PhysRevLett.107.187602>

[41] G.B. Stephenson and M.J. Highland, Equilibrium and stability of polarization in ultrathin ferroelectric films with ionic surface compensation. *Phys. Rev. B*, **84**, 064107 (2011). <https://doi.org/10.1103/PhysRevB.84.064107>

[42] S.M. Yang, A.N. Morozovska, R. Kumar, E.A. Eliseev, Y. Cao, L. Mazet, N. Balke, S. Jesse, R. Vasudevan, C. Dubourdieu, S.V. Kalinin. Mixed electrochemical-ferroelectric states in nanoscale ferroelectrics. *Nat. Phys.* **13**, 812 (2017). <https://doi.org/10.1038/nphys4103>

[43] V.A. Shchukin and D. Bimberg. Spontaneous ordering of nanostructures on crystal surfaces. *Reviews of Modern Physics*, **71**, 1125 (1999). <https://doi.org/10.1103/RevModPhys.71.1125>

[44] W. Ma. Surface tension and Curie temperature in ferroelectric nanowires and nanodots. *Appl. Phys. A* **96**, 915 (2009), <http://dx.doi.org/10.1007/s00339-009-5246-7>

[45] W. Ma. Surface tension and Curie temperature in ferroelectric nanowires and nanodots (Erratum). *Appl. Phys. A* **96**, 1035 (2009), <https://doi.org/10.1007/s00339-009-5316-x>

[46] A. N. Morozovska, E. A. Eliseev, Y. M. Fomichov, Yu. M. Vysochanskii, V. Yu. Reshetnyak, and D. R. Evans. Controlling the domain structure of ferroelectric nanoparticles using tunable shells. *Acta Materialia*, **183**, 36-50 (2020) <https://doi.org/10.1016/j.actamat.2019.11.012>

[47] See Supplementary Materials for material parameters and calculation details, URL will be provided by Publisher

---

[48] E. A. Eliseev, A. N. Morozovska, S. V. Kalinin, and D. R. Evans. Strain-Induced Polarization Enhancement in BaTiO<sub>3</sub> Core-Shell Nanoparticles. *Phys.Rev. B*. **109**, 014104 (2024);  
<https://doi.org/10.1103/PhysRevB.109.014104>

[49] H. S. Park, J. C. Shin, K. Do Kim, S. Jae Shin, J. Hee Song, S. Kyu Ryoo, I. Soo Lee, S. Hyun Lee, H. Nam, C. Seong Hwang. Enhancing ferroelectric properties of Hf<sub>0.5</sub>Zr<sub>0.5</sub>O<sub>2</sub> thin films using the HfN/TiN and W/TiN bi-layer bottom electrodes. *Journal of Materomics*, **11** (6), 101109 (2025);  
<https://doi.org/10.1016/j.jmat.2025.101109>

[50] <https://www.wolfram.com/mathematica>

[51] L. D. Landau, E. M. Lifshitz. *Theory of Elasticity* (Pergamon Press, London 1970).